

Collective variable discovery in the age of machine learning: reality, hype and everything in between

Soumendranath Bhakat^{*,†}

[†]*Division of Biophysical Chemistry, Center for Molecular Protein Science, Department of Chemistry, Lund University, P.O. Box 124, SE-22100 Lund, Sweden*

[‡]*Department of Biochemistry and Molecular Biophysics, Washington University, School of Medicine, St. Louis, United States*

E-mail: bhakat@wustl.edu/bhakatsoumendranath@gmail.com

Phone: +1-3054932620

Abstract

Understanding kinetics and thermodynamics profile of biomolecules is necessary to understand their functional roles which has a major impact in mechanism driven drug discovery. Molecular dynamics simulation has been routinely used to understand conformational dynamics and molecular recognition in biomolecules. Statistical analysis of high-dimensional spatiotemporal data generated from molecular dynamics simulation requires identification of few low-dimensional variables which can describe essential dynamics of a system without significant loss of informations. In physical chemistry, these low-dimensional variables often called *collective variables*. Collective variables are used to generate reduced representation of free energy surface and calculate transition probabilities between different metastable basins. However the choice of collective variables is not trivial for complex systems. Collective variables ranges from geometric

criteria's such as distances, dihedral angles to abstract ones such as weighted linear combinations of multiple geometric variables. Advent of machine learning algorithms led to increasing use of abstract collective variables to represent biomolecular dynamics. In this review, I will highlight several nuances of commonly used collective variables ranging from geometric to abstract ones. Further, I will put forward some cases where machine learning based collective variables were used to describe simple systems which in principle could have been described by geometric ones. Finally, I will put forward my thoughts on artificial general intelligence and how it can be used to discover and predict collective variables from spatiotemporal data generated by molecular dynamics simulations.

Keywords: collective variable, dimensionality reduction, machine learning, molecular dynamics, enhanced sampling.

Introduction

Over the past three decades, the major focus of structural biology and biophysics has been to understand conformational dynamics of biological systems across a broad range of timescales with high spatial resolution (ability to visualise molecular motion). Molecular dynamics (MD) simulation acts as a computational microscope which can capture biologically relevant conformational dynamics across varied timescales with high spatial resolution (*1*). Major advances in computational hardwares and algorithms led to an ever-growing use of MD simulation in varied biological systems. A typical MD simulation generates high-dimensional spatiotemporal data which captures complex molecular motions. Simulation of increasingly larger molecules at ever increasing time scales leads to the ‘curse of dimensionality’ which can be summarised as follows: “as the size of the biomolecule and the simulation length increases, it also increases the number of explanatory temporal variables (e.g. H-bond distances, radius of gyration, RMSD, dihedral angles etc.) and the problem of structure discovery using temporal variables gets harder. This is analogous to the problem of variable selection during

model fitting in machine learning (2).”

Capturing low-dimensional representation¹ from high-dimensional temporal data is an *open* area of research in biomolecular simulation. An excellent example of this is the large scale flap dynamics in plasmepsin-II and BACE-1 (3). In plasmepsin-II, the *sine/cos* transformation of χ_1 and χ_2 angles of 20 residues present in the flap region generates 58 dimensions. Such high number of dimensions makes it incredibly difficult to capture *slow* degrees of freedom which dominates flap *opening*. However, careful analysis of the probability distributions showed that *flipping* of χ_1 and χ_2 angles² of conserved tyrosine (Tyr) governs the flap dynamics in plasmepsin-II and BACE-1 (4). Such low-dimensional projections which best captures the conformational changes are known as collective variables (CVs) or order parameters³. Temporal evolution along CVs provide thermodynamic and kinetic informations about conformational changes (5–7). It is worth mentioning that the use of *buzz-word* “automatic identification” to highlight *new* methods for CV discovery from MD simulation gives a false impression i.e selection of good CV is a streamlined and well-defined process. But in practice, naive application of automated methods leads to uninterpretable and poor choice of CVs. Further such methods are not necessarily *new*, but in most cases direct applications or minor modifications of machine learning algorithms developed for classification (binary classifiers and their variants), signal processing (PCA, TICA, autoencoders etc), time-series prediction (neural networks, hidden Markov model etc.) and natural language processing (LSTM, transformers) etc. Recent years saw a sharp rise in applying machine learning algorithms for CV selection on systems which can be represented by simple geometric CVs e.g. dihedral angles, H-bond, RMSDs etc (highlighted in later sections).

Due to overuse of the words ‘AI/machine learning’ and flood of papers reporting new algorithms, the current field of CV discovery in biomolecular simulation is hard to navigate for a beginner or people from other disciplines. In this review we will classify the CV discovery

¹without significant loss of information regarding slow conformational degrees of freedom

²from 58 to 4 dimensions

³not to be confused with NMR order parameter which is a measure of conformational entropy

process as following: 1) geometric (dihedral angles, H-bonds, RMSD etc) and 2) abstract (PCA, ICA, neural network etc.). One question that is still up in the air: “Has the field of CV discovery in biomolecular simulation reached a plateau?”. I will provide my opinion on the aforementioned question and will put forward some challenges in order to the test the robustness and general applicability of CV discovery algorithms in context of biomolecular simulation.

Metastability & collective variables

Before we dive into the definition of CV, we must understand the concept of *metastability*. Let’s consider basic pancreatic trypsin inhibitor (BPTI) as an example and focus on a particular H-bond between *Ile18 – N – O – Tyr35* (Fig 1). In crystal conformation the aforementioned H-bond remains in a *closed* conformation. If one performs a short MD simulation, the stationary probability distribution fluctuates around the closed basin, however, careful analysis of 1 *ms* MD simulation showed formation of *broken* conformations. A CV (in this case the H-bond distance) should be able to distinguish the metastable states (such as broken and closed conformations) and estimate apparent free energy profile along it as described by following equation:

$$F(\mathbf{x}) = -k_B T \ln P(\mathbf{x}) \tag{1}$$

where \mathbf{x} is the CV of choice.

The *rugged* nature of biomolecular energy landscape is by definition characterised by numerous metastable basins. An *optimal* CV is the one for which two metastable states are separated by high free energy barrier (Figure 2). In most cases a single CV is not enough to capture the complexity of conformational landscape. Selection of CVs is an essential step to perform free energy/kinetics calculations and drive pathway based sampling methods e.g. metadynamics (8), steered MD (9), umbrella sampling (10) etc.

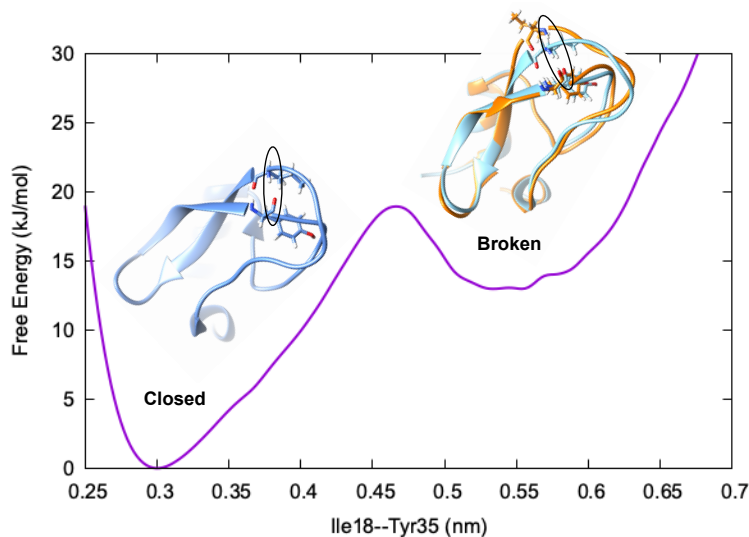


Figure 1: Free energy surface along Ile18–Tyr35 H-bond distance showing two metastable states, closed (blue) and broken (orange) in BPTI. The backbone atoms involved in hydrogen bonding are highlighted in black circle.

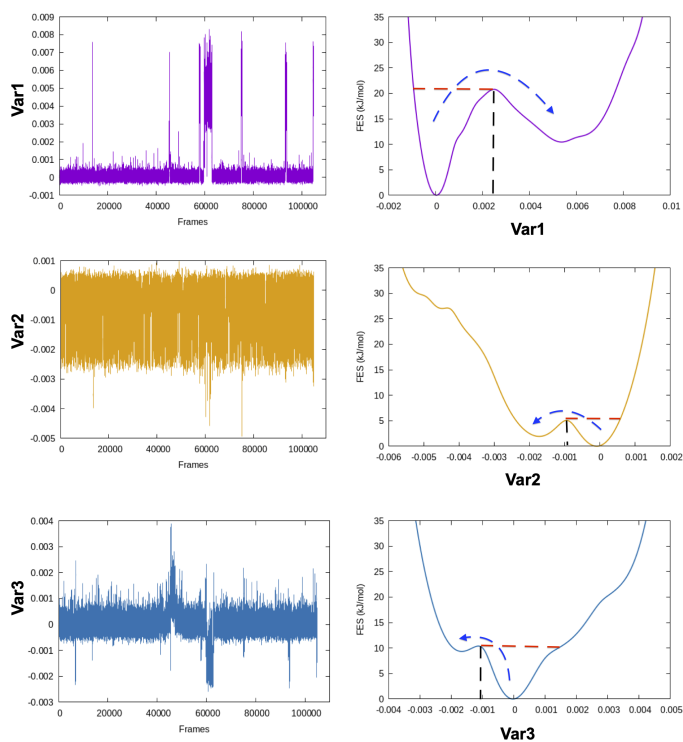


Figure 2: Fluctuation of three different variables and their corresponding free energy surfaces highlighting the differences in free energy barrier. One can see that the barrier along **Var1** is significantly higher compared to other two variables. Heuristically if one has to choose an optimum CV from these three variables, **Var1** will be the CV of choice.

For the sake of simplicity CVs can be divided into two categories: 1) geometric and 2) abstract.

Geometric CVs

Most commonly used geometric CVs that captures conformational dynamics in biomolecules are:

- a) Distance: In biomolecular simulation two kinds of distances are most commonly used:
 - i) distance between two atoms
 - ii) distance between center of mass (COM) of two group of atoms.

Distance as CVs can be used as an input within adaptive sampling and enhanced sampling methods. For example, distance between COM of ligand and protein can be used as a CV to capture ligand unbinding using well-tempered metadynamics (4, 11). Similarly H-bond distance can be used as CV (Fig 3) to capture transition between closed and broken states. Such CV can be especially useful to study transient solvent exposure in protein which leads to hydrogen-deuterium exchange (paper in preparation).

b) Switching function: A smoother version of distance CV is *switching* function (SF) which allows a smoother transition between two metastable states along a particular distance (Fig 3). A typical mathematical form⁴ of SF can be described as follows:

$$s(r) = \frac{1 - \left(\frac{r-r_{ij}}{r_0}\right)^n}{1 - \left(\frac{r-r_{ij}}{r_0}\right)^m} \quad (2)$$

where r is the instantaneous distance between atoms i and j and r_{ij} is the minimum distance between atoms i and j . For $r < r_{ij}$, $s = 1.0$ while $r > r_{ij}$ the function decays smoothly to 0 (zero). r_0 is the value of distance where $s = 0.5$. n and m are the hyper-parameters which decides the steepness of the function.

⁴other functional forms of switching function includes *tanh*, Gaussian, exponential, cubic etc.

A more general CV which combines multiple distances with switching function is known as *contact map*. It calculates the distances between a number of pairs of atoms and convert each distance by a switching function. Such CVs are useful where fluctuation along multiple distances governs conformational dynamics.

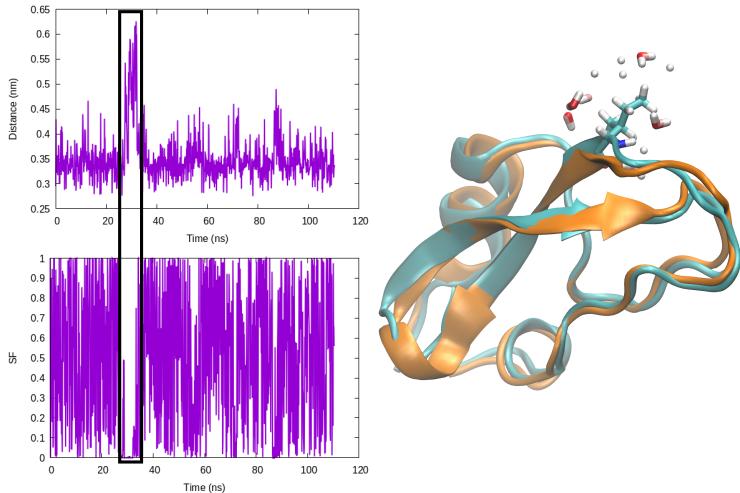


Figure 3: Temporal evolution of H-bond distance of Ile18–Tyr35 and corresponding switching function ($r_{ij} = 0.32, r_0 = 0.06, n = 6, m = 12$) in BPTI. CV values corresponding broken H-bond conformations is highlighted in black square. Snapshot corresponding broken conformation highlights how breaking of H-bond leads to solvent exposure (highlighting water molecules within 3 Å radius of Ile18) of Ile18-NH.

c) Dihedral angle: Tracking temporal evolution of dihedral angles (e.g. $\phi, \psi, \omega, \chi_1, \chi_2$) during MD simulation is a well established method to capture conformational dynamics of biomolecules. Most common example includes tracking the conformational sampling in alanine dipeptide by probability distribution along ϕ and ψ angles. Recently, *Bhakat and Söderhjelm* (4) showed that the conformational dynamics of pepsin-like aspartic proteases can be captured by two dihedral angles⁵: χ_1 and χ_2 angles of conserved Tyr (Fig 4 highlights evolution of χ_1 during molecular dynamics simulation). However in many cases, conformational dynamics of biomolecules can't be captured by a few dihedral angles. In complex cases, linear combinations of dihedral angles (more on this later) can be used as CVs to capture biomolecular dynamics.

⁵way to measure similarity between two dihedral CV is to use a function $s = \frac{1}{2} \sum_i [1 + \cos(\chi_1 - \chi_2)]$

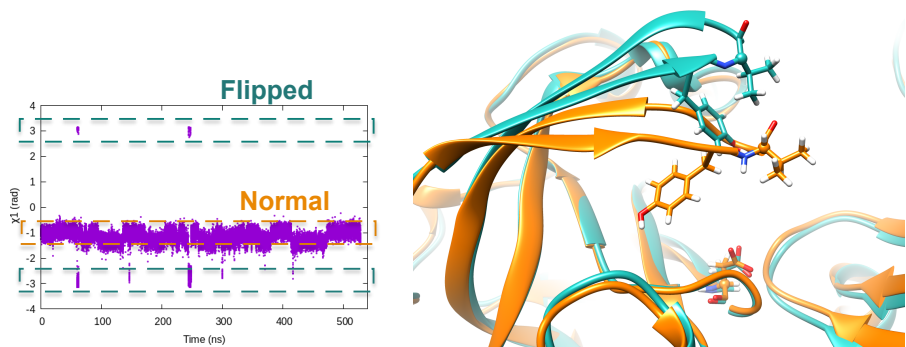


Figure 4: Time-series projection of χ_1 angle of Tyr77 in plasmepsin-II during unbiased molecular dynamics simulation (PDB: 1LF4). Tyr77 predominantly remains in the *normal* state (orange) with rare sampling of the *flipped* state (blue). Conformational snapshots corresponding normal and flipped states with relative position of flap (β hairpin structure), flap tip residue Val78 and catalytic Asp34 is also highlighted. In plasmepsin-II, rotation of Tyr77 along χ_1 and χ_2 angles dictates the extent of flap opening which governs substrate entry and catalytic activity.

d) RMSD: RMSD is one of the commonly used CV which measures the similarity between two superimposed atomic co-ordinates. RMSD is the measure of average distance and in bimolecular simulation it measures deviation of atomic co-ordinates from the starting conformation using the following equation:

$$RMSD = \sqrt{\frac{1}{n} \sum_{i=1}^n d_i^2} \quad (3)$$

where d_i is the distance between atom i and a reference structure. RMSD is usually calculated for $C\alpha$ /backbone atoms of the entire protein or for a specific subset. *Stock and coworkers* argued that RMSD is not an optimal choice to capture local conformational (e.g. loop dynamics, domain motions etc.) changes at long-timescales (12). In our unpublished study we have shown that RMSD analysis on a carefully chosen subset can able to capture conformational changes at longer timescales (Figure 5). RMSD based CVs can be used within enhanced sampling and adaptive sampling frameworks to accelerate sampling of the conformational space.

where χ_1 and χ_2 are the dihedral angles and their corresponding instantaneous values.

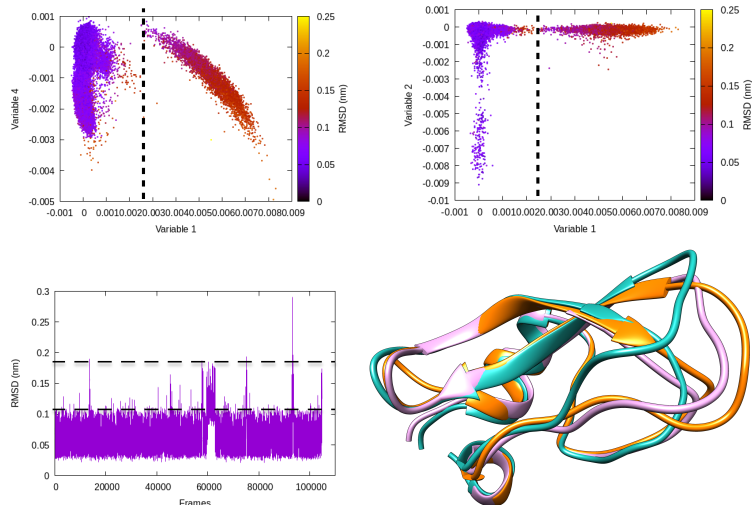


Figure 5: Projection of different variables (more precisely time independent components as described in Figure 8) which captures transient loop opening BPTI as a function of $C\alpha$ RMSD of residue 6 – 56 in BPTI. It can be easily seen that a higher RMSD value separates two metastable states along variable 1. Snapshots corresponding crystal (orange), RMSD \sim 0.15 nm (pink) and RMSD \sim 0.25 nm (sea green) highlights differences in loop conformation. RMSD calculation was performed on $M1$ state (13) of 1 ms long conventional MD simulation performed by D.E. Shaw research (14).

Besides the aforementioned CVs, several other geometric variables (radius of gyration, $eRMSD$) are frequently used to analyse MD simulations. Softwares e.g. *Plumed* (15), *gmx* plugins integrated with Gromacs, *CPPTRAJ* (16), *MDAnalysis* (17), *MDTraj* (18) have build-in capabilities to perform analysis of MD trajectories using geometric CVs.

Abstract CVs

Abstract CVs are usually linear or non-linear transformations of geometric CVs (e.g. dihedral angles, distances, RMSD etc). However the former is often less *intuitive* compared to the latter. In case of linear transformation, the transformed data is a linear combination of original variables. Whereas non-linear transformations are more complex than that. In this section, I will underscore some of abstract CVs (**linear**: principal component analysis & independent component analysis; **non-linear**: *kernel* trick, diffusion map, t-SNE) that have been regularly used to capture low-dimensional spatiotemporal representation from

high dimensional dataset generated by MD simulation. I will further discuss the probabilistic interpretation of variational autoencoders which has been applied to capture compressed representation of temporal variables from molecular simulation. Finally, I will highlight the application of binary classifiers in context of classifying metastable states and drive enhanced sampling simulations to capture state transitions. I will further list the softwares/tools/codes that can be used to generate abstract CVs in context of biomolecular simulation.

Principal Component Analysis

Principal component analysis (PCA) is an unsupervised dimensionality reduction method which transforms a set of variables $r_1, r_2, r_3, \dots, r_N$ (where $\mathbf{r} = [r_1, r_2, \dots, r_N]^T$) to low dimensional representations y_i which captures as much of the variations as possible. It has been widely used by biomolecular simulation community to capture molecular motions with largest amplitude (high variance) citepca1,pca2,pca3. Let $\mathbf{r} \in \mathbb{R}^D$ be a vector of geometric CVs e.g. dihedral angles or distances⁶. *First* principal component (PC1) of the dataset $r_1, r_2, r_3, \dots, r_N$ is the weighted linear combination of the features that captures the largest variance:

$$y_1 = w_{11}r_1 + w_{21}r_2 + w_{31}r_3 + \dots + w_{N1}r_N \tag{4}$$

where w_1 is the vectors of weights or coefficients⁷ with elements $w_{11}, w_{21}, \dots, w_{N1}$. The elements are normalised i.e. $\sum_{i=1}^N w_{i1}^2 = 1$. The process of generating PCs can be summarised as follows:

- a) generate a *mean free* version of the input data i.e. a vector of geometric CVs.
- b) compute *eigenvectors* and *eigenvalues* from the covariance matrix

$$\mathbf{C} = \frac{1}{N} \hat{\mathbf{r}}^T \hat{\mathbf{r}} \tag{5}$$

⁶assuming r is mean free

⁷PCA aims to find w which maximises the variance

where $\hat{\mathbf{r}}$ is the mean free version of \mathbf{r} .

c) sort the eigenvalues in descending order and retain k (k is the new subspace $k < D$) eigenvectors that corresponds to k largest eigenvalues. The eigenvector corresponds to the largest eigenvalue capture the greatest variability in the data.

d) construct a projection matrix \mathbf{w} with elements w_{1j}, w_{2j}, w_{Nj} (where $\mathbf{w} = [w_{1j}, w_{2j}, \dots, w_{Nj}]^T$).

e) generate the PCs, \mathbf{y} by transforming the original geometric vectors \mathbf{r} via elements of the projection matrix \mathbf{w} .

Principal components are *uncorrelated* to each other (as eigenvectors are *orthogonal* to one another) and sorted by their variance ($PC1 > PC2 > PC3 \dots$). PCs extracted from MD dataset defines direction in feature space along maximal variance (largest amplitude/fluctuations). PCA has been applied routinely on periodic (dihedral angles⁸) and non-periodic (CA atomic positions, RMSDs, distances) degrees of freedom (Fig 6). The coefficients w corresponding each variables allows incorporating PCs as CVs within enhanced sampling protocols e.g. metadynamics and its variants. PCA reduced dimensions can be also used to construct free energy surface of biomolecules. Despite its success, application of PCA in biomolecular simulation has been a subject of controversy. It has been argued that PCA can't capture the slow conformational degrees of freedom within time scales accessible to MD simulations. However, the author believes that PCA on a carefully chosen subset of atomic co-ordinates⁹ can capture slow conformational changes in biomolecules.

Softwares: *MDAnalysis*, *Plumed* (with capability of using PCs as CVs in metadynamics), *MSMBuilder* (19), *PyEMMA* (20), *pytraj*, *scikit-learn* (can't be directly used on MD trajectories but can be interfaced with MD post-processing tools e.g. *MDTraj*).

⁸using *sin* and *cos* transformation

⁹still an open question and requires further study

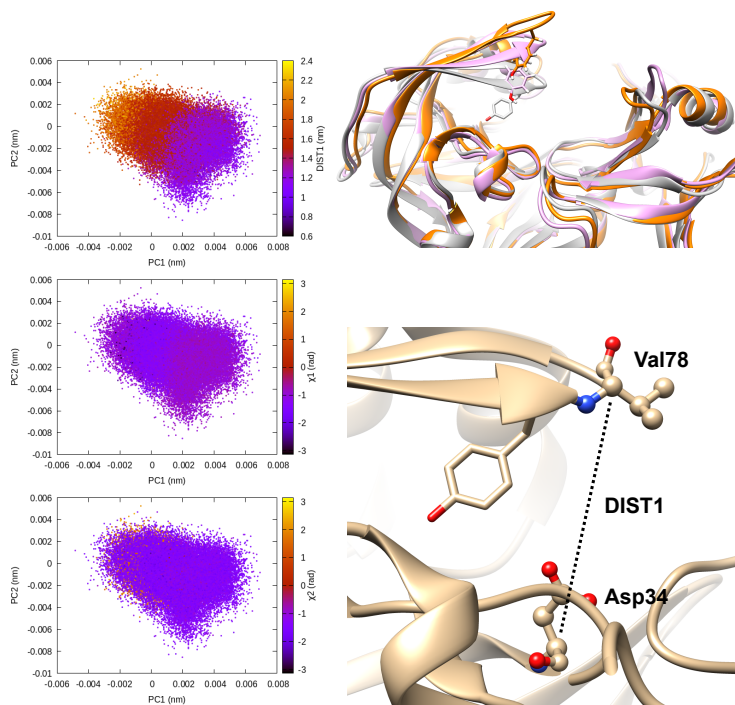


Figure 6: Principal components project along $C\alpha - C\alpha$ distance ($DIST1$) between Asp34-Val78 and χ_1 and χ_2 angles of flap tip Tyr77 in plasmepsin-II. One can see that PCs managed to capture the extent of flap opening which is quantified by $DIST1$ ($DIST1 > 1.8nm$ is open conformation). In this case PCA analysis was performed on the the $C\alpha$ atoms of the protein hence it is unable to capture rotational degrees of freedom along χ_1 and χ_2 angles. Conformational snapshots corresponding crystal (grey, $DIST2 = 1.2nm$), semi-open (magenta, $DIST1 = 1.6nm$) and open conformation (orange, $DIST1 = 2.0nm$) are also highlighted.

Independent Component Analysis

Independent component analysis is a dimensionality reduction method which transforms a set of vectors (e.g distances, RMSDs, dihedral angles etc.) into maximally independent linear combinations (independent components). Imagine $\mathbf{y}(t) = [y_1(t), \dots, y_N(t)]^T$ is a linear mixture of high-dimensional data $\mathbf{r}(t) = [r_1(t), \dots, r_N(t)]^T$ ¹⁰ such that $\mathbf{y}(t) = \mathbf{A}\mathbf{r}(t)$ where \mathbf{A} is the square mixing matrix and the components of $\mathbf{y}(t)$ are mutually independent. Two components can said to be independent if their joint distribution is equal to the product

¹⁰data is mean free

of their marginals¹¹:

$$p(y_1(t), y_2(t)) = p(y_1(t))p(y_2(t)) \quad (6)$$

where $p(y_1(t), y_2(t))$ are the joint probability distributions and $p(y_1(t))p(y_2(t))$ is the marginal along two components $y_1(t)$ and $y_2(t)$. However the aforementioned definition of independence has a drawback: lets consider a signal without time auto-correlation and a second signal which is equal to the first signal but shifted in time (often known as signal with time-delay). If one applies equation 6 the two signals will appear to be mutually independent. The time-delayed signal can be called statistically independent if all the time-delayed correlations are zero (second-order ICA) (21). In biomolecular simulation second-order ICA is known as time-lagged independent component analysis (TICA) (22, 23). The first step of second-order ICA/TICA is to introduce a time-lagged (or time-delayed) correlation matrices of the input variables $\mathbf{r}(t)$:

$$\mathbf{C}^r(\tau) = \langle \mathbf{r}(t)\mathbf{r}(t+\tau)^T \rangle \quad (7)$$

where τ is the lag-time or time delay between two signals. The entries of $\mathbf{C}^r(\tau)$ ¹² are denoted as $\mathbf{C}_{ij}^r(\tau)$. The common practice is to express $\mathbf{C}^r(\tau)$ as a symmetrized version of correlation matrices:

$$\mathbf{C}^r(\tau) = \frac{1}{2} [\langle \mathbf{r}(t)\mathbf{r}(t+\tau)^T \rangle + \langle \mathbf{r}(t+\tau)\mathbf{r}(t)^T \rangle] \quad (8)$$

Symmetrization is a mathematical trick which allows applying the algorithm to the reversible dynamics (as $\langle \mathbf{r}(t+\tau)\mathbf{r}(t)^T \rangle = \langle \mathbf{r}(t)\mathbf{r}(t-\tau)^T \rangle$). It also makes sure that the eigenvalues are *real* and two eigenvectors that comes from distinct eigenvalues are *orthogonal*. Finally the TICA problem can be formulated a generalised eigenvalue problem¹³:

$$\mathbf{C}^r(\tau) \mathbf{A} = \mathbf{C}^r(0) \mathbf{A} \mathbf{\Lambda} \quad (9)$$

¹¹a corresponding measure of independence is Kullback-Leibler divergence

¹²should be diagonal for all τ

¹³can be solved by second-order blind source separation algorithms e.g. AMUSE

where $\mathbf{A} = (a_1, \dots, a_N)$ is the orthogonal matrix of generalised eigenvectors and $\mathbf{\Lambda} = \text{diag}(\lambda_1, \dots, \lambda_N)$ is the diagonal matrix of eigenvalues¹⁴. \mathbf{A} contains the independent components (ICs) the original data $\mathbf{r}(t)$ can be projected on the TICA space as: $\mathbf{y}(t) = \mathbf{A}\mathbf{r}(t)$. The scalar components of λ_i captures the magnitude of the auto-covariance where smaller λ_i captures largest auto-covariance:

$$\lambda_1 < \lambda_2 < \dots < \lambda_N; \lambda_1 \text{ captures largest auto-covariance and so on} \quad (10)$$

The eigenvalues, λ_i are associated with the relaxation timescales of a biomolecular process by:

$$t_i = -\frac{\tau}{\ln |\lambda_i|} \quad (11)$$

TICA has been routinely used on temporal data from molecular dynamics simulation to identify slow conformational degrees of freedom such as flipping of side-chain dihedral angle (Figure 7), transient exposure of protein interior which leads of solvent exposure (Figure 8) and drive enhanced sampling simulations (24). Recently Schultze and Grubmuller compared projection of TICs between high-dimensional data from protein dynamics and random walk (25). However the authors disregarded any discussion surrounding the choice of input features and its effect on TICA. Figure 7 highlights the importance of input features in describing conformational dynamics along TIC space. Lack of *separation aka population gap* along TIC space in ref (25) (see Figure 7, left panel) is a sign that either TICA analysis was performed on a poorly chosen feature space or the sampling was not sufficient enough to capture slow conformational dynamics in proteins.

Wiskott and co-workers (26) have shown how the objective function of TICA with lag time 1 is formally equivalent to *slow feature analysis* (SFA)¹⁶ (Figure 9). SFA and TICA are based on two different principles: *slowness* and *statistical independence*. However, the similarity between SFA and TICA (second order ICA with lag-time 1) opens up possibilities

¹⁴the eigenvalues $\lambda_1, \dots, \lambda_N$ are associated with eigenvectors of a_1, \dots, a_N .

¹⁶captures slowly varying features from high-dimensional input

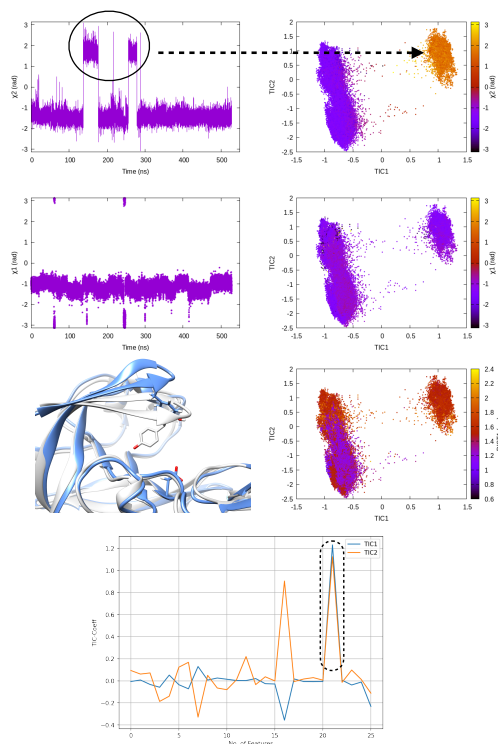


Figure 7:

Evolution of χ_1 and χ_2 angles of Tyr77 of plasmepsin-II during MD simulation. TICA analysis¹⁵ was performed on χ_1 and χ_2 angles (*sin/cos* modification) of residue 74-84. Projection of TIC1 and TIC2 along χ_1 and χ_2 angles of Tyr77 shows that TIC1 managed to capture the slowest degree of motion which is the χ_2 rotation of Ty77. Further, projection along TICs failed to separate fluctuation along DIST1 as it is defined by distance between backbone $C\alpha$ atoms. Fluctuation of TIC coefficients (eigenvalues) also highlights feature no 21 (*sin χ_2* of Tyr77) as the dominant feature among 25 features (Table 1 in Supplementary Informations). Snapshots corresponding crystal (grey) and flipped ($\chi_2 \sim 2$ rad) are also highlighted.

to combine these two algorithms (27) for capturing *slowly varying statistically independent* components from high-dimensional temporal data generated by MD simulation.

Softwares: *MSMBuilder* (19), *PyEMMA* (20) and *deeptime* (29) comes with built in TICA functionality. A scikit-learn style implementation of SFA can be found here: <https://github.com/wiskott-lab/sklearn-sfa>.

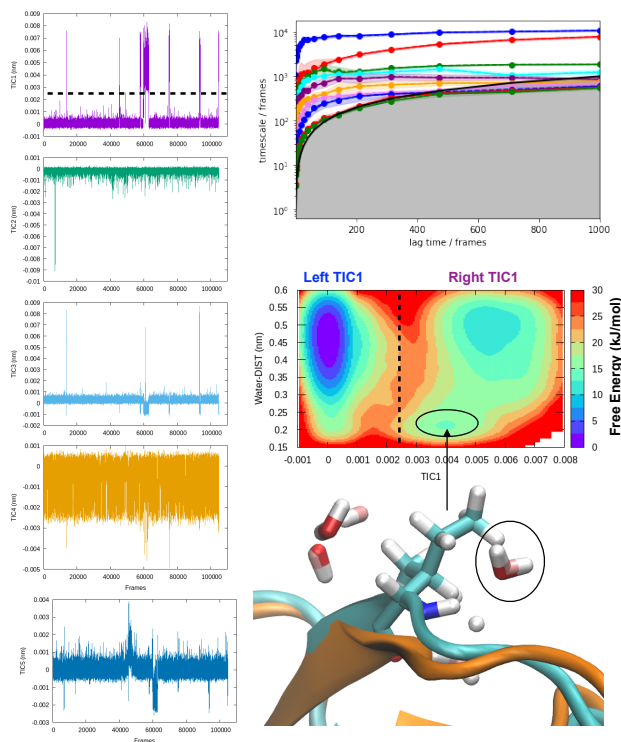


Figure 8: Time-series projection of first 5 TICs and corresponding implied timescales showing how first few TICs captured slow conformational degrees of freedom (transient loop opening as depicted in Figure 5) in BPTI. TICA analysis was performed on $C\alpha$ atomic positions of residues 6 – 56 using a lag time 500 (all calculations were performed on M1 state as described by ref (13)). Transient loop opening in BPTI leads to breaking of H-bod interaction between *Ile18 – NH* and *Tyr35 – O* which makes the amide of *Ile18* solvent exposed and enables hydrogen-deuterium exchange (28). Projection of water distance from *Ile18 – NH* shows how TIC1 captures a metastable solvent exposed basin where a water molecule comes within 0.25 nm of amide hydrogen. Snapshot corresponding solvent exposed conformation highlights the relative position of backbone amide and closest (with 0.3 nm) waters.

Kernel trick

MD simulation generates complex and non-linear representation of biomolecular dynamics. *Kernel* trick is a mathematical transformation which maps the original data into a higher dimensional feature space which is then used to find linear projections using PCA (kernel PCA) or tICA (kernel TICA (30)). For data points r_i, r_j in the input space \mathbb{N} , kernel function $k(r_i, r_j)$ generates modified inner products which maps $\mathbb{N} \rightarrow \mathbb{Z}$

$$k(r_i, r_j) = \langle \phi(r_i), \phi(r_j) \rangle_{\mathbb{Z}} \quad (12)$$

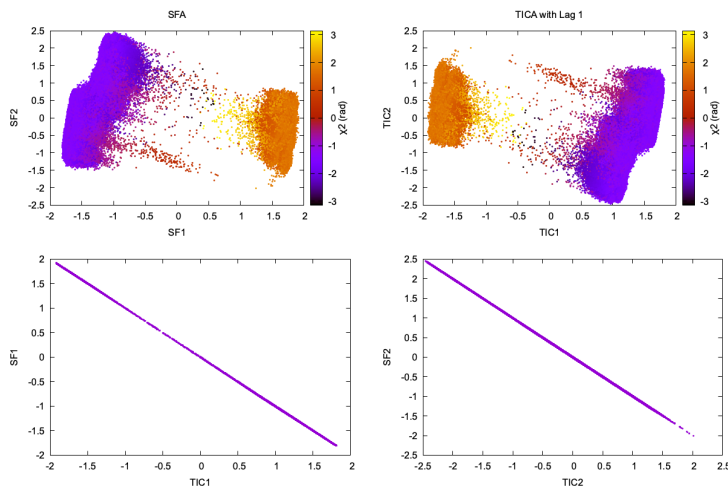


Figure 9: Projection of slow features and TICs with lag time 1 along χ^2 angle of Tyr77 shows similarity of TICA and SFA in separating slow conformational degree of freedom. The squared Pearson correlation coefficient, R^2 between SFA and TICA with lag time 1 is 1.00. This example is a demonstration of mathematical concepts described in ref (26) in context of biomolecular simulation. It further raises possibilities of combining the two algorithms and use it to develop Markov state model.

where ϕ is the mapping function and $\langle \cdot, \cdot \rangle_{\mathcal{Z}}$ must be proper inner product. One doesn't need to explicitly compute ϕ as the kernel matrix $k(r_i, r_j)$ (modified inner product) can be easily computed by a variety of functions:

- a) *Polynomial* kernel: $k(r_i, r_j) = (\gamma \cdot r_i^T r_j + c)^d, \gamma > 0$
- b) *Sigmoid* kernel: $k(r_i, r_j) = \tanh(\gamma \cdot r_i^T r_j + r)$
- c) *Gaussian* kernel: $k(r_i, r_j) = \exp(-\gamma \cdot \|r_i - r_j\|^2), \gamma > 0$

where r , d and γ are kernel hyper-parameters. A drawback of this approach is that when we map the data into higher dimensions, we may overfit the model. Hence the choice of right kernel functions are of utmost importance. Schwartz and colleagues used kernel PCA (using polynomial kernel function) to identify CVs in lactate dehydrogenase. Further, kernel TICA has been used to identify CVs which captures folded to unfolded transition in small folded proteins (31).

Softwares: *scikit-learn* and *MODE-TASK* (32) have in-built kernel PCA functionality. *MSMBuilder* has a built in kernel TICA algorithm which can be applied on high-dimensional

features from MD dataset for discovering low-dimensional representations *aka* CVs.

Diffusion Map

Diffusion map is a non-linear dimensionality reduction technique. It combines the concept of random walk Markov chain and diffusion process by projecting the input data in a low-dimensional space where the distance (e.g Euclidean) between data points resembles the diffusion distance in the original high-dimensional space. When applied to MD dataset, diffusion map generated vector space (CVs) are constructed in such a way that conformations which are kinetically closed are placed together whereas kinetically distant (separated by high free-energy barrier) conformations are placed far apart.

In a random walk Markov model the connectivity between data points r_i and r_j is defined as the probability of jumping from state r_i to r_j in one step of random walk. The connectivity can be also expressed as a normalised kernel function $k(r_i, r_j)$ ¹⁷ which measures similarity between data points:

$$\begin{aligned} k(r_i, r_j) &= \exp(-\gamma \cdot \|r_i - r_j\|^2), \gamma > 0 \\ &= \exp\left(-\frac{\|r_i - r_j\|^2}{\alpha}\right) \end{aligned} \tag{13}$$

where the value of α decides the size of neighbourhood. It can also be seen as a hyper-parameter which chooses the conformations that are kinetically closed. In practice conformations closer than the value of α are relevant for $k_{ij} = k(r_i, r_j)$ as the contribution from distant conformations decays exponentially. The diffusion kernel satisfies the following two properties:

- a) k is symmetric: $k(r_i, r_j) = k(r_j, r_i)$. This allows spectral analysis of the distance matrix k_{ij}
- b) $k(r_i, r_j) \geq 0$.

¹⁷similar functional form of Gaussian kernel. One can choose other measures of distances as kernel functions e.g. Mahalanobis distance, Jensen-Shannon divergence etc.

The transition probability $p(r_i, r_j)$ can be expressed as:

$$p(r_i, r_j) = \frac{1}{D}k(r_i, r_j) \quad (14)$$

where D is the normalisation factor. The normalised transition matrix \mathbf{P} with $P_{ij} = p(r_i, r_j)$ (where $\sum_j P_{ij} = 1$) allows spectral (in other words *eigen*) decomposition:

$$\mathbf{P}\mathbf{A} = \mathbf{\Lambda}\mathbf{A} \quad (15)$$

where a_1, \dots, a_N ($\mathbf{A} = (a_1, \dots, a_N)$) are real valued eigenvectors corresponding to eigenvalues $\lambda_1, \dots, \lambda_N$ ($\mathbf{\Lambda} = \text{diag}(\lambda_1, \dots, \lambda_N)$) where $1 = \lambda_1 > \lambda_2 \dots \geq \lambda_N$. Similarly to TICA, the eigenvalues generated from normalised transition matrix \mathbf{P} shows *spectral gap* which can be expressed as the difference between two largest eigenvalues $\lambda_1 - \lambda_2$ or more generally $1 - \max\{|\lambda_2|, |\lambda_N|\}$. Diffusion map at time t can be approximated as mapping between the original space and the latent space of first k eigenvectors:

$$\mathbf{A}(\mathbf{r}) = (\lambda_1^t a_1(r), \lambda_2^t a_2(r), \dots, \lambda_k^t a_k(r)) \quad (16)$$

The diffusion distance¹⁸ at time t can be expressed as a function of eigenvectors. Kevrekidis and coworkers (34) has shown that the diffusion distance can be approximated as Euclidean distance on the diffusion map space:

$$D_t^2(r_i, r_j) = \sum_l \lambda_l^{2t} (a_l(r_i) - a_l(r_j))^2 = \|\mathbf{A}_t(r_i) - \mathbf{A}_t(r_j)\|^2 \quad (17)$$

Equation 16 provides justification of using Euclidean distance in the diffusion map space for clustering. Diffusion distance can also be interpreted as a measure of how kinetically close are the two conformations. The distance is small if there are multiple high probability transition pathways between two conformations. Diffusion map has been applied in biomolecular

¹⁸analogous to the functional form of kinetic distance as proposed by Noe and Clementi ref (33)

simulation to capture *slow* transitions and guide enhanced sampling simulations (35–37). Recently the functional form of equation 16 in combination with maximum entropy based CV selection method SGOOP¹⁹ was used to capture kinetically relevant low dimensional projection in small peptides (38).

Softwares: MDAAnalysis has an integrated diffusion map module which can be applied on selected features from MD simulation.

t-distributed stochastic neighbour embedding

t-distributed stochastic neighbour embedding (t-SNE) is a non-linear dimensionality reduction method which performs embedding of high-dimensional data to low-dimensional space such that neighbouring data-points are assigned highest probability while distant points are assigned lower probability (39, 40). For a high-dimensional space r_1, \dots, r_N the distance between r_j and r_i can be expressed as:

$$p_{j|i} = \frac{\exp(-\|r_i - r_j\|^2 / 2\sigma_i^2)}{\sum_{k \neq i} \exp(-\|r_i - r_k\|^2 / 2\sigma_i^2)} \quad (18)$$

where $p_{j|i}$ is the conditional probability which captures the similarity between data points r_j with r_i such that $p_{i|i} = 0$ and $\sum_j p_{j|i} = 1$. The functional form of equation 18 is similar to Gaussian kernel in equation 13. The conditional probability can be transformed into a joint probability distribution of symmetrized matrix P_{ij} :

$$P_{ij} = \frac{p_{j|i} + p_{i|j}}{2N} \quad (19)$$

where $P_{ij} = P_{ji}$, $P_{ii} = 0$ and $\sum_{i,j} P_{ij} = 1$.

The Gaussian bandwidth σ_i has been set in such a way that the perplexity of the conditional distribution equals to the perplexity provided by the user²⁰. The perplexity is defined

¹⁹in principal one can use the same strategy to combine diffusion distance with TICA/SFA

²⁰ref (39) highlighted that there is a monotonically increasing relationship between perplexity and bandwidth

as:

$$Perp(p_i) = 2^{H(p_i)} \tag{20}$$

where p_i is the conditional probability distribution over all the data-points given r_i and $H(p_i)$ is the Shannon entropy $H(p_i) = -\sum_j p_{j|i} \log_2 p_{j|i}$. Perplexity can be thought as a measure of nearest neighbours and the choice of perplexity heavily determines the outcome of t-SNE (Figure 10).

t-SNE aims to learn a low dimensional manifold r'_1, \dots, r'_N in such a way that the new conditional probability $p'_{j|i}$ reflects similarity with $p_{j|i}$. $p'_{j|i}$ can be expressed as:

$$p'_{j|i} = \frac{(1 + \|r'_i - r'_j\|^2)^{-1}}{\sum_{l \neq k} (1 + \|r'_k - r'_l\|^2)^{-1}}, p'_{i|i} = 0 \tag{21}$$

The distance based metrics $(1 + \|r'_i - r'_j\|^2)^{-1}$ is a heavily tailed distribution. In t-SNE, Student t-distribution has been used to measure the similarity between low-dimensional data-points so that the points that are far apart have $p'_{j|i}$ which are invariant of perturbation. The algorithm aims to minimise the *Kullback-Leibler* divergence²¹ (using gradient descent) by comparing joint probability distributions P' (low-dimensional) and P (high-dimensional):

$$KL(P||P') = \sum_{i \neq j} p_{ij} \log \frac{p_{ij}}{q_{ij}} \tag{22}$$

The gradient descent algorithm is usually effective for small datasets but performs poorly in case of larger datasets. Recently a time-lagged version of t-SNE (41) was proposed using inspiration from time-lagged ICA (TICA). However, the stochastic nature (mainly due to *perplexity*) of t-SNE (as shown in Figure 10 and discussed in ref (42)) prevents its use as a meaningful CV for reconstructing trustworthy free energy surface and calculating kinetics from MD simulation²². Clustering on the top of t-SNE embedding can also produce artificial

²¹other measures of similarity e.g. Jensen-Shannon divergence, Bhattacharya distance can be explored to improve the embedding result

²²recently proposed feed forward neural network based tSNE otherwise known as parametric t-SNE can also be applied on MD dataset

clusters which might trick the user of thinking that it discovers new metastable states but in reality they belong to the same free energy basin.

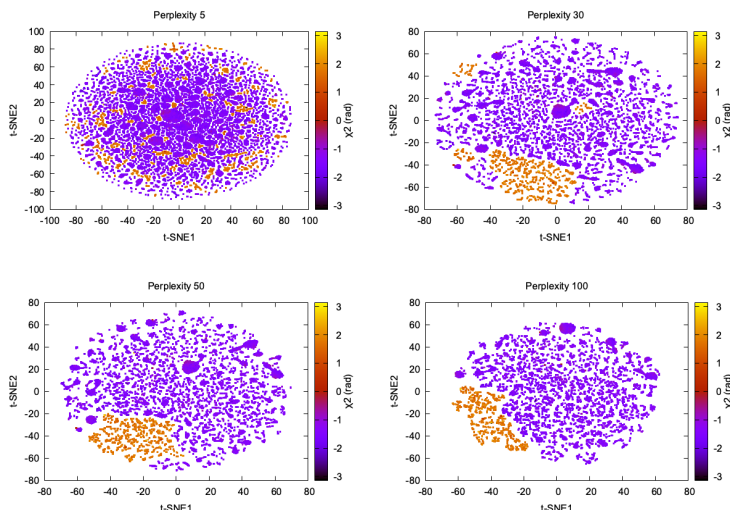


Figure 10: Projection of first two t-SNE components along χ_2 angle of Tyr77 in plasmepsin-II shows how the embedding changes with perplexity. Further t-SNE performed on the high dimensional torsional features (Table 1 in supplementary informations) didn't manage to separate flipping along χ_2 which is a slow degree of freedom. It further shows that clustering on top of t-SNE reduced dimensions will generate artificial clusters which in reality belong to same metastable state.

Softwares: Time-lagged version of t-SNE can be accessed here: <https://github.com/spiwokv/tltsne>. Popular machine learning package *scikit-learn* also has a t-SNE module: <https://scikit-learn.org/stable/modules/generated/sklearn.manifold.TSNE.html>. MODE-TASK <https://github.com/RUBi-ZA/MODE-TASK> a python toolkit for analysing MD simulation has an integrated t-SNE functionality. Tensorboard embedding projector <https://projector.tensorflow.org> has a graphical user interface to perform t-SNE.

In recent years, several other dimensionality reduction methods such as spectral gap optimization of order parameters (SGOOP) (43), isomap (44) (<https://scikit-learn.org/stable/modules/generated/sklearn.manifold.Isomap.html>), dynamic mode decomposition (DMD) (45) (<https://mathlab.github.io/PyDMD/>, see ref (46) for similarity between DMD and TICA and their variants), multi-dimensional scaling (MDS) (44), UMAP (47, 48) (<https://umap-learn.readthedocs.io/en/latest/>, Figure 11), iVIS (49) (<https://umap-learn.readthedocs.io/en/latest/>,

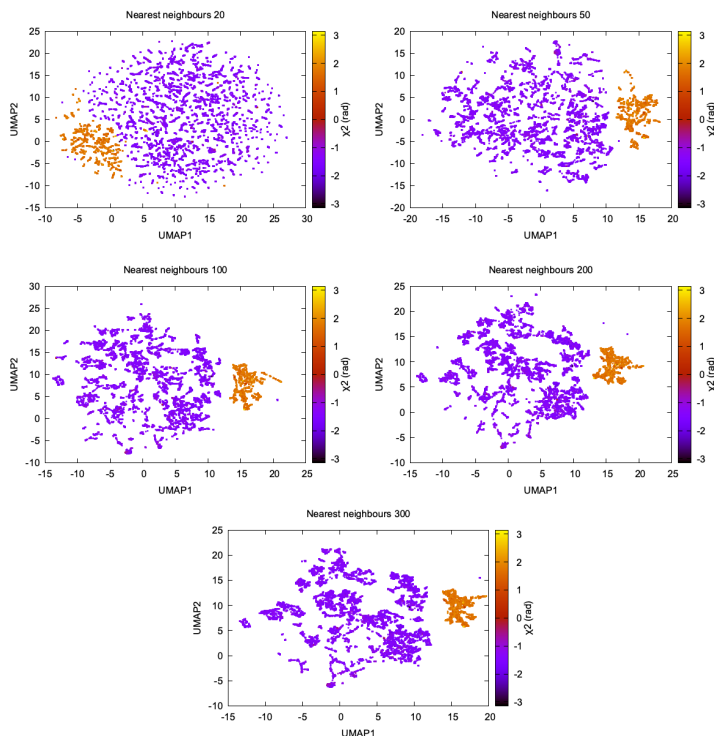


Figure 11: UMAP components projected along χ^2 of Tyr77 highlights how the shape of UMAP vary as a function of *nearest neighbour* hyper-parameter. UMAP converges with nearest neighbour 200. UMAP does a better job compared to t-SNE in separating conformational space along χ^2 . I believe clustering on top of UMAP reduced dimensions might be useful in understanding conformational heterogeneity within a broad metastable basin.

([//bering-ivis.readthedocs.io/en/latest/](http://bering-ivis.readthedocs.io/en/latest/)) which are similar to some of the aforementioned algorithms, were applied on temporal data from MD simulation. Further, *sparse regression* based dimensionality reduction method *sparse identification of nonlinear dynamical systems* (SINDy) (50) can possibly be applied on temporal data from molecular dynamics simulation to discover linear combinations of features which best captures conformational dynamics in macromolecules. Recent review by *Glielmo et al* (51) summarises mathematical concepts, strengths and limitations as well as applicability of few such methods in analysing high-dimensional data from MD simulations.

Learning co-ordinates for dynamics using variational autoencoder

Variational autoencoder (VAE) is a dimensionality reduction method which takes high dimensional data (e.g multi-variate geometric or abstract CVs) as inputs and learns latent (compressed) representations that captures minimal essential information necessary to describe the dynamics of the system. VAE is a type of autoencoder whose principals are deeply rooted in *variational* statistics (52, 53). In this article we will use the language of *probability theory* to describe VAE and try to establish a connection between free energy and the *loss function* of VAE.

VAE takes high dimensional vector $\mathbf{r} = [r_1, r_2, \dots, r_N]^T$ as inputs. Each components of \mathbf{r} are probability distributions along geometric or abstract CVs. The encoder part of the VAE encodes the high dimensional data into the latent variables \mathbf{z} . The joint probability distribution of input and latent variables, $p(r, z)$ can be expressed as:

$$p(r, z) = p(r|z) p(z) \tag{23}$$

The generative process can be expressed as:

- a) sampling latent variables, z_i from the prior distribution $p(z)$ and
- b) sampling of data point r_i from the likelihood $p(r|z)$ which is conditional on the latent variables z .

The goal of VAE is to infer good approximation of the latent variables (z) given input data (r) which is equivalent to calculate the posterior distribution $p(z|r)$ as following:

$$p(z|r) = \frac{p(r|z) p(z)}{p(r)} = \frac{p(r, z)}{p(r)} \tag{24}$$

where

$$p(r) = \int p(r|z) p(z) dz \tag{25}$$

Estimation of $p(r)$ is a computationally expensive process as it requires integrating over all the possible values of z . VAE approximates the posterior distribution $p(z|r)$ by a new distribution $q(z|r)$ (tractable distribution). If $q_\lambda(z|r)$ is similar to $p(z|r)$ then we can use it to approximate $p(r)$. λ is the hyper-parameter which indicates type of distribution. If $q(z|r)$ a Gaussian distribution then $\lambda_{r_i} = (\mu_{r_i}, \sigma_{r_i}^2)$ where μ is the mean and σ^2 is the variance of latent variables of each input component.

Now we want to measure how well $q_\lambda(z|r)$ approximates $p(z|r)$. VAE uses Kullback-Leibler (KL) divergence to measure information loss between two probability densities as described below:

$$\begin{aligned}
KL(q_\lambda(z|r)||p(z|r)) &= \mathbb{E}_q \left[\log \frac{q_\lambda(z|r)}{p(z|r)} \right] \\
&= \mathbb{E}_q [\log q_\lambda(z|r) - \log p(z|r)] \\
&= \mathbb{E}_q [\log q_\lambda(z|r)] - \mathbb{E}_q [\log p(r, z)] + \log p(r); \text{ taking } \log \text{ of eq. 24} \\
&= -(\mathbb{E}_q [\log p(r, z)] - \mathbb{E}_q [\log q_\lambda(z|r)]) + \log p(r) \\
&= -ELBO(\lambda) + \log p(r)
\end{aligned} \tag{26}$$

We can reformulate equation 26 as follows:

$$\log p(r) = ELBO(\lambda) + KL(q_\lambda(z|r)||p(z|r)) \tag{27}$$

From equation 27 we can see that minimising KL divergence (KL divergence is always greater or equal to zero) is equivalent to maximising Evidence Lower Bound (ELBO). It allows us to bypass the hard task of minimising KL divergence between the approximate $q(z|r)$ and true posterior $p(z|r)$, instead we maximise ELBO. ELBO term can be further expressed as follows:

$$\begin{aligned}
ELBO(\lambda) &= \mathbb{E}_q [\log p(r, z)] - \mathbb{E}_q [\log q_\lambda(z|r)] \\
&= \mathbb{E}_q [\log p(r|z)] + \mathbb{E}_q [\log p(z)] - \mathbb{E}_q [\log q_\lambda(z|r)]; \text{ log transformation of eq. 23} \\
&= \mathbb{E}_q [\log p(r|z)] - KL(q_\lambda(z|r)||p(z))
\end{aligned} \tag{28}$$

Equation 28 is known the VAE loss function (L):

$$L = \mathbb{E}_q [\log p(r|z)] - KL(q_\lambda(z|r)||p(z)) \leq \log p(r) \quad (29)$$

In biomolecular simulation deep neural network (DNN) encodes input data and computes λ which approximates $q_w(z|r, \lambda)$. The decoder takes $p(z)$ as input and maps into original distribution $p_{w'}(r|z)$. w and w' acts as a neural network weights. w transforms the input data within the neural network hidden layers and the resulting latent variable is a combination of linear transformations that are modified by non-linear activation functions. Weights are learnable parameters during VAE training. The value of weight dictates the importance of a variable. A higher weight value corresponding an input component indicates that it will have a significant influence on the output.

Mathematically speaking, the reason behind VAE's popularity in biomolecular simulation community is due to the interconnectivity between *loss function* and variational free energy (F):

$$\begin{aligned} KL(q_\lambda(z|r)||p(z|r)) &= \int q_\lambda(z|r) \log \frac{q_\lambda(z|r)}{p(z|r)} dz \\ &= \int q_\lambda(z|r) \log \frac{q_\lambda(z|r)p(r)}{p(r, z)} dz \\ &= \int q_\lambda(z|r) \log \frac{q_\lambda(z|r)}{p(r, z)} dz + \int q_\lambda(z|r) \log p(r) dz \\ &= \int q_\lambda(z|r) \log \frac{q_\lambda(z|r)}{p(r, z)} dz + \log p(r); \text{ as } \int q_\lambda(z|r) dz = 1 \\ &= - \int q_\lambda(z|r) \log \frac{p(r, z)}{q_\lambda(z|r)} dz + \log p(r) \\ &= -F + \ln p(r) \end{aligned} \quad (30)$$

where

$$\int q_\lambda(z|r) \log p(r) dz = 1 \quad (31)$$

By comparing equation 26 with 31 we can conclude that the variational free energy (F) is equal to the $ELBO(\lambda)$. Thus minimising KL divergence is equivalent to maximising the

variational free energy (F).

Figure 12 shows a typical architecture of VAE in context of biomolecular simulation. The encoder part of the VAE acts as a non-linear dimensionality reduction of input \mathbf{r} . Whereas the decoder DNN acts an input reconstruction. VAE has been primarily used a dimensionality reduction method to compress multi-variate probability distributions. The weights of the encoder layer which maps the input data onto the latent layer has been further used to drive enhanced sampling simulations such as metadynamics (54). As the latent layer of VAE represents a non-linear combination of input data hence it reduces the need of multiple CVs as inputs in metadynamics (traditionally metadynamics is limited to a maximum of two CVs). However in terms of exploration of the conformational space, metadynamics bias applied to multiple CVs²³ (parallel-bias metadynamics) will be equivalent to using VAE’s latent variable as CV in a 1D metadynamics. Several different flavours of VAEs have been developed which mainly differs in their architecture (e.g β -VAE²⁴ which uses an additional hyper-parameter β to learn disentangled latent variables by controlling the KL divergence (55)) and types of inputs (e.g VAE-SNE which takes output of tSNE as inputs, DMD-VAE which can take multiple dynamic modes as inputs, SINDy-VAE which takes outputs from SINDy algorithm as inputs). In future, different variants of VAE can be applied on molecular dynamics simulation to capture conformational heterogeneity and drive enhanced sampling calculations.

Softwares & implementations: VAEs for post-processing high-dimensional time-series data generated from MD simulation can be implemented using popular machine learning libraries e.g PyTorch, Tensorflow, Keras etc. Recently Pande and co-workers (56)(variational dynamic encoder: <https://github.com/msmbuilder/vde>) as well as Tiwary and colleagues (57) (RAVE: <https://github.com/tiwarylab/RAVE>) applied VAE to compress high-dimensional temporal data and able to capture non-linear dynamics in context

²³each of them as an input in VAE

²⁴possible future application in biomolecular simulation to compare encoding representation difference with traditional VAE

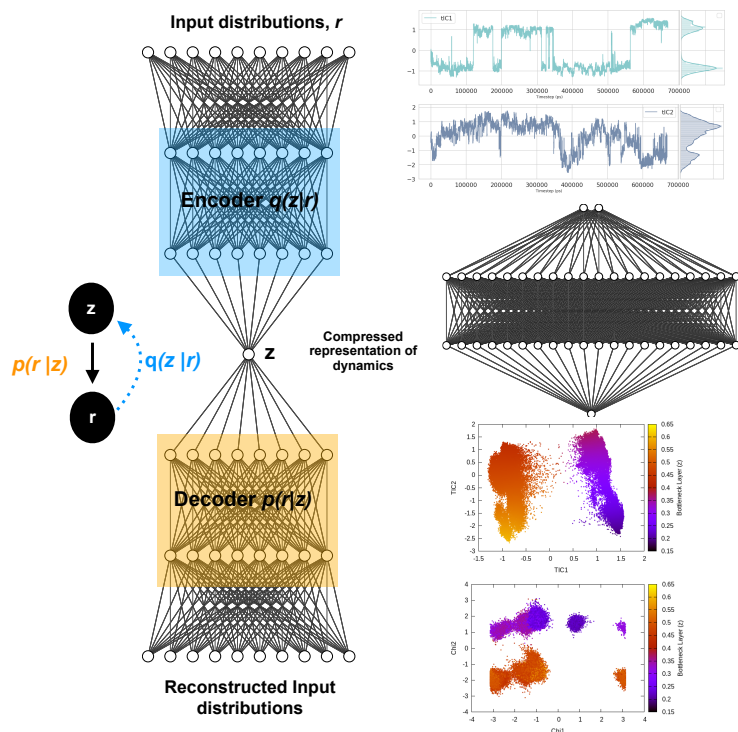


Figure 12: Left panel showing a typical architecture of deep neural network based variational autoencoder. The input distributions r can be probability distributions of geometric variables, TICs, DMD etc. Right panel shows how latent layer of variational autoencoder learned the dynamics of the system using TICs as inputs. TICs were generated using χ_1 and χ_2 angles of residues present in the flap region of plasmepsin-II (Table 1 in supplementary informations) with lag-time 1000. Following hyper-parameters were used during the training process of VAE, no of hidden layers=2, no of neurons in each hidden layer=20, epochs=100, batch size=500, learning rate= $1e - 2$.

of protein folding, protein-ligand binding/unbinding etc. A collection of prebuilt VAE architectures implemented with PyTorch (<https://github.com/AntixK/PyTorch-VAE>) opens up the possibility to evaluate VAE variants in context of molecular dynamics simulation.

Classifiers as CVs

Classifiers are supervised learning algorithms which uses feature vectors and feature values to map input data into specific categories (58). In molecular dynamics simulation, the classifiers are used as CVs to recognise different metastable states²⁵ based on a common set

²⁵can also be used to identify features that distinguishes wild and mutant variants

of feature values that distinguishes them (Figure 13). Recently different classes of classifiers (e.g. support vector machine, logistic regression, artificial neural network, linear discriminant analysis etc.) have been applied to categorise different metastable states and drive enhanced sampling simulations (59, 60). In this article, I will discuss support vector machine (SVM) and linear discriminant analysis (LDA) and their applications in enhanced sampling.

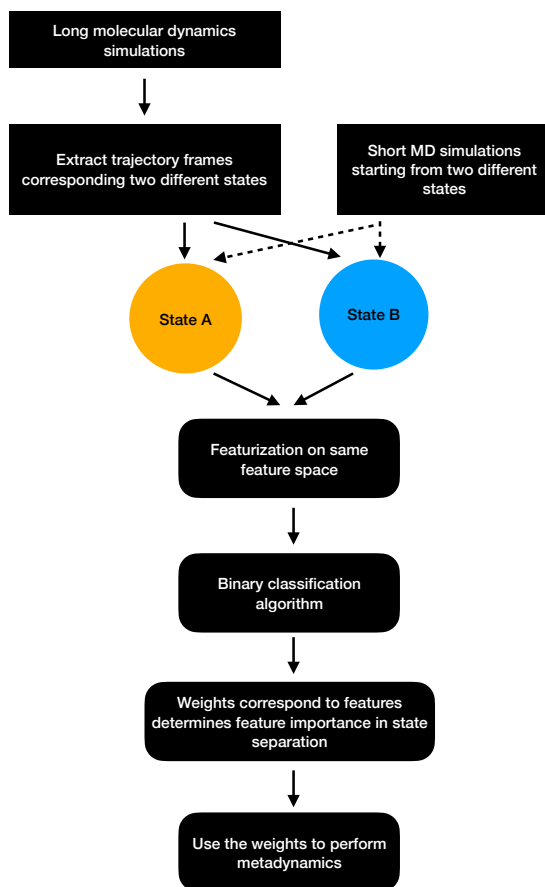


Figure 13: Schematic representation of showing how binary classifiers can be used to separate metastable states and drive enhanced sampling calculations.

Support vector machine:

Let A and B are two metastable states which can be represented by unique points in space where each point belongs to high-dimensional feature vector $\mathbf{r} = [r_1, \dots, r_N]$. The goal of SVM algorithm is to find a separating hyperplane that maximises the minimum distance between closest points (support vectors) of the two metastable states (otherwise known as

classes):

$$d_H = \frac{\mathbf{w}^T \mathbf{r} + b}{\|\mathbf{w}\|_2} \quad (32)$$

where d_H is the distance of a point to hyperplane, \mathbf{w} is the vector of coefficients²⁶, b is the intercept and $\frac{1}{\|\mathbf{w}\|_2}$ is the normalisation term. The SVM algorithm then maximise the minimum distance $w^* = \arg_w \max[\min_n d_H]$. In context of biomolecular simulation, equation 32 acts a CV which can separate metastable states and drive enhanced sampling²⁷ simulations (Figure 14). Sultan and Pande showed how d_H can be used as CV within metadynamics framework to sample conformational space of alanine dipeptide and chignolin folding (59). SVM algorithm can be further extended for non-linear classification by using *kernel* trick as explained before.

Linear Discriminant Analysis:

Linear discriminant analysis (LDA) is a supervised dimensionality reduction method which finds linear combinations of features that best separates two or more metastable states (62). Imagine two metastable states with common features \vec{r} have means $\vec{\mu}_A$ and $\vec{\mu}_B$ and covariances Σ_A and Σ_B . The linear combinations of features $\vec{w} \cdot \vec{r}$ (\vec{w} is known as LDA coefficients) will have means $\vec{w} \cdot \vec{\mu}_{A,B}$ and variances $\vec{w}^T \Sigma_{A,B} \vec{w}$. LDA objective function separates two distributions by taking ratio between variance between the classes to variance within classes:

$$s(LDA) = \frac{(\vec{w} \cdot (\vec{\mu}_B - \vec{\mu}_A))^2}{\vec{w}^T (\Sigma_A + \Sigma_B) \vec{w}} \quad (33)$$

Mathematically it can shown that the maximum separation occurs when $\vec{w} \propto \frac{(\vec{\mu}_B - \vec{\mu}_A)}{(\Sigma_A + \Sigma_B)}$. LDA algorithm can be generalised to more than one classes (Multi-class LDA). Equation 33 acts as a CV in metadynamics to drive transition between state A and B . Recently Parrinello and co-workers used a harmonic version of LDA (HLDA) as a CV to study folding of a small protein and protein-ligand binding/unbinding (60, 63). The framework of LDA can be patched with neural network (Deep-LDA) as well as *kernel* trick in order to introduce non-

²⁶it's direction gives us the predicted class: positive or negative

²⁷multiple metastable states can also be classified by SVM CV followed by parallel-bias metadynamics

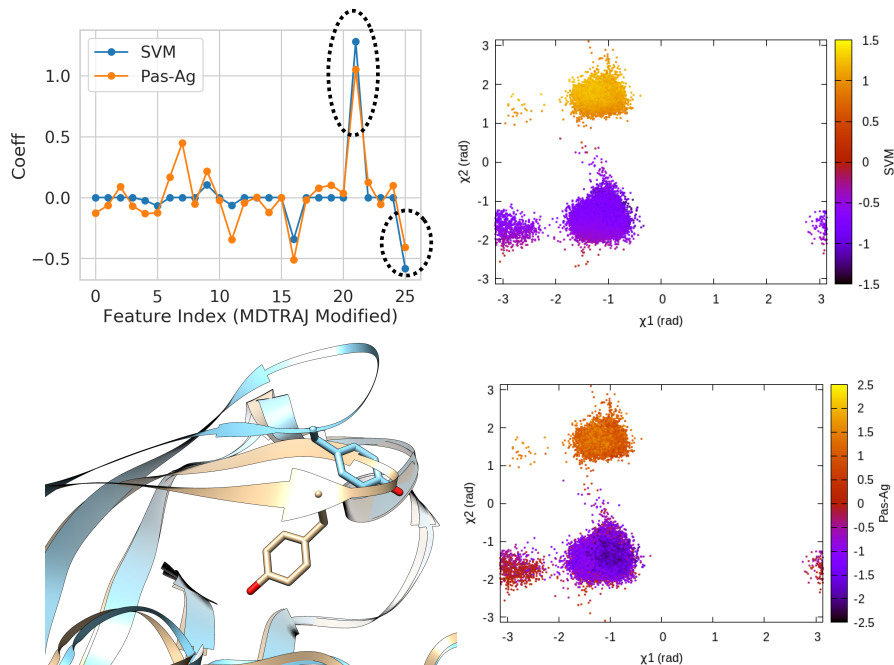


Figure 14: Coefficients (weights) correspond to linear SVM and passive aggressive classifier(61) trained on χ_1 and χ_2 angles of residue 74-84 (Table 1 in Supplementary Informations) in plasmepsin-II showing the importance of $\sin\chi_2$ (feature 21) and $\cos\chi_2$ (feature 25) in separating two metastable basins, normal ($\chi_2 \sim -1$ rad) and flipped ($\chi_2 \sim 2$ rad). 50 ns trajectories from each basins were used for training purpose using the scheme described in Figure 13. Further χ_1 and χ_2 angles of Tyr77 projected along classifier decision boundaries demonstrated separation of metastable states. Snapshots corresponding normal (grey) and flipped (blue) states are also highlighted.

linearity. Recently Deep-LDA framework has been applied in SAMPL5 host-guest systems to accurately calculate binding free energy and to understand the role of water molecule in ligand binding (64).

In order to apply classifier algorithms to separate metastable states one first need to sample different metastable states. However, sampling of metastable states separated by high entropic barrier often requires ultra-long MD simulations or enhanced sampling simulations e.g. parallel-tempering. Further, one needs to carefully choose a set of features that can separate a set of metastable states. For complex systems, selection of such features are not trivial and often needs significant amount of trial and error.

Softwares: *scikit-learn's* supervised learning module incorporates both LDA and SVM

algorithms for training purpose. It further integrates various other supervised learning algorithms that can be applied to classify metastable states and act as CVs in enhanced sampling simulations.

Algorithms to predict temporal evolution of CVs: proposing a challenging dataset

Recently neural network based time-series prediction models such as long short-term memory (LSTM) and transformers were proposed to predict rare events and extract kinetics and thermodynamics (65, 66). These methods often work quite well on simpler systems where the training data has multiple recrossing. However in order to correctly predict kinetics from time-series one first needs to accurately predict the frequency and lifetime of rare events. In case of figure 15, temporal evolution along H-bond and dihedral angle CVs showed multiple recrossing whereas evolution along TIC1 only captures transient recrossing between metastable states. Intuitively one can say predicting temporal evolution along TIC1 (*rare* fluctuation) is far more challenging task when compared with H-bond or dihedral angle. No such study is currently available which compares the time-series prediction capability of neural networks in context of different CVs. In future, such study is necessary to understand the limit of neural network based time-series prediction algorithms (67) in terms of capturing temporal evolution of *rare* events.

Softwares: Tiwary and co-workers (65) used LSTM based neural network to predict temporal evolution in model systems. Their code can be accessed here: <https://github.com/tiwarylab/LSTM-predict-MD>.Tensorflow (<https://www.tensorflow.org/text/tutorials/transformer> and <https://www.tensorflow.org/guide/keras/rnn>) and Pytorch (<https://github.com/jdb78/pytorch-forecasting>) based time-series forecasting modules can be used for this purpose. Zeng and co-workers (66) used LSTM/transformers to predict temporal evolution of different CVs in alanine dipeptide (<https://github.com/Wendysigh/LSTM-Transformer-for-MD>).

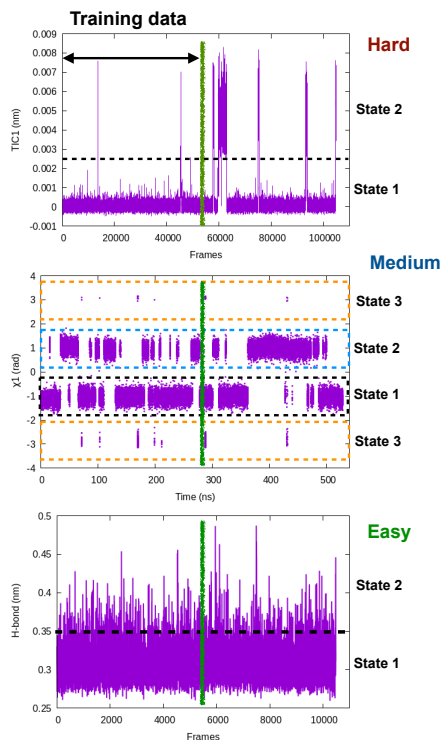


Figure 15: Pictorial representation showing time-series fluctuation of different CVs and their hypothetical prediction difficulty using LSTM, transformers style neural network. Along H-bond distance one can see multiple recrossing between two states which makes it an *easy* case for time-series prediction algorithms. In case of dihedral flipping along χ_1 , training data observes several recrossing between state 1 and 2 however, there are transient sampling of rare transitions to state 3 which makes it a *medium* level difficult task. In case of TIC1, the training data contains rare transitions between state 1 and 2 hence I believe it will be a *hard* task for time-series prediction algorithms. One way to compare time-series projection results along a CV is compare mean first passage transition time (MFPT) as well as lifetime of different states with temporal data from long MD simulation.

Use of machine learning/AI in CV selection: The Hype

Recently numerous papers reported different combinations of abstract order parameters to capture conformational dynamics and molecular recognition of macromolecules. In one such case neural network based LDA (Deep-LDA) approach has been applied on SAMPL5 host-guest systems to estimate binding free energy (64). Previously funnel metadynamics using simple distance CV combined with artificial restraint along binding-site solvation managed to accurately predict the binding free energy for the same host-guest systems (68). We can ask

a question: was deep-LDA framework necessary for a relatively simple problem such as host-guest binding/unbinding which was previously solved using simple geometric CVs? One can argue that deep-LDA framework is more natural as it didn't impose any artificial restraint along solvent degrees of freedom. In SAMPL5 host-guest systems, the solvation (when the binding site is occupied by long-lived water molecule) of the binding site is a slow process (Figure S2 in ref (68)). In principal TICA/SGOOP (which by design capable of capturing slow degrees of freedom) could have solved such a problem. Further, deep-LDA method is a slightly fancier application of previously described work which uses binary classifiers as CVs to drive conformational sampling (59). This is a classic example where the developers of a CV discovery method used buzzwords to solve a trivial problem without pointing out how exactly such deep learning based CV is superior compared to other geometric or abstract order parameters.

In another case authors used TICs/SGOOPs as inputs within a VAE and used the VAE's latent layer as CV for enhanced sampling (54, 69). Such an approach is advantageous if an enhanced sampling method is limited to driving along one CV. Further, the eigenvalues corresponding each TIC/SGOOP can be used to filter geometric CVs which then can be used as an input in VAE. This approach can be seen as an extension of previous approach where one inputs TICs/SGOOPs directly into VAE. However a critic can ask: is there any advantage in terms of sampling if one uses VAE's latent layer vs multiple CVs²⁸ within metadynamics (Figure 16) and more importantly can you call such method artificial intelligence (AI)?.

Most of the algorithms described in the previous section either require extensive sampling or previous knowledge about metastable states in order to capture conformational changes in biomolecules. These algorithms can be best described as data driven machine learning algorithms which solves a deterministic closed set finite problems using large amount of training data. An *near-term* artificial general intelligence (AGI) on other hand will learn about the dynamical system on the fly without the external supervision (e.g feature selection,

²⁸using parallel-bias metadynamics

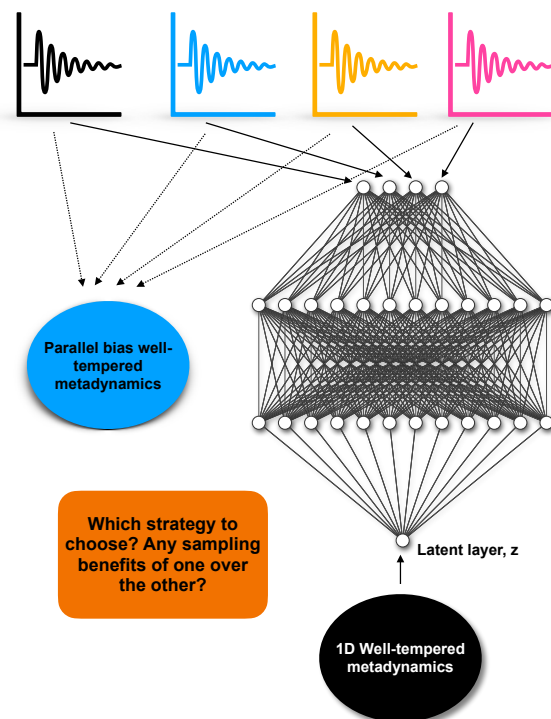


Figure 16: Describes dilemma of choosing an enhanced sampling strategy over other: in case of four different CVs (depicted by black, blue, yellow and magenta) one can either choose to perform a parallel-bias (70) variant of well-tempered metadynamics simulation or feed these four CVs within variational autoencoder and uses the latent layer of variational autoencoder as CV in 1D well-tempered metadynamics.

choice of algorithms, tuning of hyper-parameters etc) and extract observables that can be confirmed by biophysical experiments. Development of such *self-aware* AGI will require significant innovation in terms of novel algorithms and software design. Until that time, the biomolecular simulation community should refrain from using the word AI in context of identifying low-dimensional representation to approximate kinetics and thermodynamics of biomolecular systems.

Conclusions

In recent years data-driven machine learning models impacted the field of biomolecular simulation and have been applied in context of protein folding, protein-ligand/protein binding

and capturing rare conformational changes during molecular simulation. However a real challenge in comparing the power of different machine learning models is due to absence of a common dataset. We believe that the basic pancreatic trypsin inhibitor (BPTI) can act as a reasonable dataset to test different algorithms. The reasons behind that are accessibility of a) 1ms long MD simulation and b) experimental observables such as NMR order parameter, kinetics of ring flipping (rare events) and protection factors (measure of amide hydrogen-deuterium exchange). Further transient loop opening of BPTI which leads to amide hydrogen-deuterium exchange (28) and aromatic ring flipping (71, 72) are the rare events that can be captured by both simulation and experiments. Transient loop opening leads to amide hydrogen-deuterium exchange which is represented by a metric called protection factor. A good machine learning model for CV discovery combined with an enhanced sampling framework should sample the rare events and predict experimental observables (rate of ring flipping and protection factors). Recent metadynamics based investigation with geometric CVs (dihedral angles) highlighted the challenge of sampling *slow* ring flipping in BPTI. In order to live up to the hype, machine learning based abstract CVs should do better in sampling such rare events and predict kinetics.

A major leap forward in combining machine learning with molecular dynamics will be prediction of multi-dimensional spatiotemporal evolution of biomolecular dynamics. Recently, transformer network has been applied to model crowd motion dynamics which managed to achieve state-of-the-art performance on commonly used pedestrian prediction datasets (73). In future extension of such work can be applied in context of molecular dynamics simulation to predict temporal evolution of CVs and corresponding spatial representation²⁹. However prediction of spatiotemporal evolution of biomolecular structure without correctly capturing the water dynamics doesn't model physical reality as water plays integral role in molecular recognition and conformational dynamics of biomolecules. We hope breakthroughs in quantum computer together with novel machine learning algorithms will make spatiotemporal

²⁹such prediction will require extensive long simulations as training data

prediction of solvated biomolecular system a reality, until then we have to carefully select geometric/abstract CVs to capture dynamics of biomolecules from atomistic simulations.

Acknowledgement

The computations were performed on computer resources provided by the Swedish National Infrastructure for Computing (SNIC) at LUNARC (Lund University) and HPC2N (Umeå University). The author thanks Borna Novak for carefully reading the manuscript.

Conflicts of Interest

Author declares no potential conflicts of interest.

Supporting Information Available

Supplementary informations contain tables and link to Github which can be used to replicate calculations performed in this study.

References

1. Hollingsworth, S. A., and Dror, R. O. (2018) Molecular Dynamics Simulation for All. *Neuron* *99*, 1129–1143.
2. Fan, J., and Lv, J. (2010) A Selective Overview of Variable Selection in High Dimensional Feature Space. *Statistica Sinica* *20*, 101–148.
3. Bhakat, S. (2021) Pepsin-like aspartic proteases (PAPs) as model systems for combining biomolecular simulation with biophysical experiments. *RSC Adv.* *11*, 11026–11047.
4. Bhakat, S., and Söderhjelm, P. (2020) Flap dynamics in pepsin-like aspartic proteases: a computational perspective using Plasmepsin-II and BACE-1 as model systems. *bioRxiv*
5. Bussi, G., and Laio, A. (2020) Using metadynamics to explore complex free-energy landscapes. *Nature Reviews Physics* *2*, 200–212.
6. Wang, Y., Lamim Ribeiro, J. M., and Tiwary, P. (2020) Machine learning approaches for analyzing and enhancing molecular dynamics simulations. *Current Opinion in Structural Biology* *61*, 139–145.
7. Chen, M. (2021) Collective variable-based enhanced sampling and machine learning. *The European Physical Journal B* *94*, 211.
8. Valsson, O., Tiwary, P., and Parrinello, M. (2016) Enhancing Important Fluctuations: Rare Events and Metadynamics from a Conceptual Viewpoint. *Annual Review of Physical Chemistry* *67*, 159–184, PMID: 26980304.
9. Patel, J. S., Berteotti, A., Ronsisvalle, S., Rocchia, W., and Cavalli, A. (2014) Steered Molecular Dynamics Simulations for Studying Protein–Ligand Interaction in Cyclin-Dependent Kinase 5. *Journal of Chemical Information and Modeling* *54*, 470–480.

10. You, W., Tang, Z., and Chang, C.-e. A. (2019) Potential Mean Force from Umbrella Sampling Simulations: What Can We Learn and What Is Missed? *Journal of Chemical Theory and Computation* 15, 2433–2443.
11. Dodda, L. S., Tirado-Rives, J., and Jorgensen, W. L. (2019) Unbinding Dynamics of Non-Nucleoside Inhibitors from HIV-1 Reverse Transcriptase. *The Journal of Physical Chemistry B* 123, 1741–1748.
12. Sittel, F., and Stock, G. (2018) Perspective: Identification of collective variables and metastable states of protein dynamics. *The Journal of Chemical Physics* 149, 150901.
13. Persson, F., and Halle, B. (2013) Transient Access to the Protein Interior: Simulation versus NMR. *Journal of the American Chemical Society* 135, 8735–8748.
14. E., S. D., Paul, M., Kresten, L.-L., Stefano, P., O., D. R., P., E. M., A., B. J., M., J. J., K., S. J., Yibing, S., and Willy, W. (2010) Atomic-Level Characterization of the Structural Dynamics of Proteins. *Science* 330, 341–346.
15. Tribello, G. A., Bonomi, M., Branduardi, D., Camilloni, C., and Bussi, G. (2014) PLUMED 2: New feathers for an old bird. *Computer Physics Communications* 185, 604–613.
16. Roe, D. R., and Cheatham, T. E. (2013) PTRAJ and CPPTRAJ: Software for Processing and Analysis of Molecular Dynamics Trajectory Data. *Journal of Chemical Theory and Computation* 9, 3084–3095.
17. Michaud-Agrawal, N., Denning, E. J., Woolf, T. B., and Beckstein, O. (2011) MDAanalysis: A toolkit for the analysis of molecular dynamics simulations. *Journal of Computational Chemistry* 32, 2319–2327.
18. McGibbon, R. T., Beauchamp, K. A., Harrigan, M. P., Klein, C., Swails, J. M., Hernández, C. X., Schwantes, C. R., Wang, L.-P., Lane, T. J., and Pande, V. S. (2015)

- MDTraj: A Modern Open Library for the Analysis of Molecular Dynamics Trajectories. *Biophysical Journal* 109, 1528–1532.
19. Harrigan, M. P., Sultan, M. M., Hernández, C. X., Husic, B. E., Eastman, P., Schwantes, C. R., Beauchamp, K. A., McGibbon, R. T., and Pande, V. S. (2017) MSM-Builder: Statistical Models for Biomolecular Dynamics. *Biophysical Journal* 112, 10–15.
 20. Scherer, M. K., Trendelkamp-Schroer, B., Paul, F., Pérez-Hernández, G., Hoffmann, M., Plattner, N., Wehmeyer, C., Prinz, J.-H., and Noé, F. (2015) PyEMMA 2: A Software Package for Estimation, Validation, and Analysis of Markov Models. *Journal of Chemical Theory and Computation* 11, 5525–5542.
 21. Molgedey, L., and Schuster, H. G. (1994) Separation of a mixture of independent signals using time delayed correlations. *Phys. Rev. Lett.* 72, 3634–3637.
 22. Pérez-Hernández, G., Paul, F., Giorgino, T., De Fabritiis, G., and Noé, F. (2013) Identification of slow molecular order parameters for Markov model construction. *The Journal of Chemical Physics* 139, 015102.
 23. Schwantes, C. R., and Pande, V. S. (2013) Improvements in Markov State Model Construction Reveal Many Non-Native Interactions in the Folding of NTL9. *Journal of Chemical Theory and Computation* 9, 2000–2009, PMID: 23750122.
 24. M. Sultan, M., and Pande, V. S. (2017) tICA-Metadynamics: Accelerating Metadynamics by Using Kinetically Selected Collective Variables. *Journal of Chemical Theory and Computation* 13, 2440–2447, PMID: 28383914.
 25. Schultze, S., and Grubmüller, H. (2021) Time-Lagged Independent Component Analysis of Random Walks and Protein Dynamics. *Journal of Chemical Theory and Computation* 17, 5766–5776.

26. Blaschke, T., Berkes, P., and Wiskott, L. (2006) What Is the Relation Between Slow Feature Analysis and Independent Component Analysis? *Neural Computation* 18, 2495–2508.
27. Blaschke, T., and Wiskott, L. Independent Slow Feature Analysis and Nonlinear Blind Source Separation. Independent Component Analysis and Blind Signal Separation. Berlin, Heidelberg, 2004; pp 742–749.
28. Persson, F., and Halle, B. (2015) How amide hydrogens exchange in native proteins. *Proceedings of the National Academy of Sciences* 112, 10383–10388.
29. Hoffmann, M., Scherer, M., Hempel, T., Mardt, A., de Silva, B., Husic, B. E., Klus, S., Wu, H., Kutz, N., Brunton, S. L., and Noé, F. Deeptime: a Python library for machine learning dynamical models from time series data. 2021.
30. Schwantes, C. R., and Pande, V. S. (2015) Modeling Molecular Kinetics with tICA and the Kernel Trick. *Journal of Chemical Theory and Computation* 11, 600–608.
31. Harrigan, M. P., and Pande, V. S. (2017) Landmark Kernel tICA for Conformational Dynamics. *bioRxiv*
32. Ross, C., Nizami, B., Glenister, M., Sheik Amamuddy, O., Atilgan, A. R., Atilgan, C., and Tastan Bishop, Ö. (2018) MODE-TASK: large-scale protein motion tools. *Bioinformatics* 34, 3759–3763.
33. Noé, F., and Clementi, C. (2015) Kinetic Distance and Kinetic Maps from Molecular Dynamics Simulation. *Journal of Chemical Theory and Computation* 11, 5002–5011.
34. Nadler, B., Lafon, S., Kevrekidis, I., and Coifman, R. Diffusion Maps, Spectral Clustering and Eigenfunctions of Fokker-Planck Operators. Advances in Neural Information Processing Systems. 2006.

35. Zheng, W., Rohrdanz, M. A., and Clementi, C. (2013) Rapid Exploration of Configuration Space with Diffusion-Map-Directed Molecular Dynamics. *The Journal of Physical Chemistry B* 117, 12769–12776.
36. Ferguson, A. L., Panagiotopoulos, A. Z., Debenedetti, P. G., and Kevrekidis, I. G. (2010) Systematic determination of order parameters for chain dynamics using diffusion maps. *Proceedings of the National Academy of Sciences* 107, 13597–13602.
37. Ferguson, A. L., Panagiotopoulos, A. Z., Kevrekidis, I. G., and Debenedetti, P. G. (2011) Nonlinear dimensionality reduction in molecular simulation: The diffusion map approach. *Chemical Physics Letters* 509, 1–11.
38. Tsai, S.-T., Smith, Z., and Tiwary, P. (2021) SGOOP-d: Estimating Kinetic Distances and Reaction Coordinate Dimensionality for Rare Event Systems from Biased/Unbiased Simulations. *Journal of Chemical Theory and Computation* 17, 6757–6765.
39. van der Maaten, L., and Hinton, G. (2008) Visualizing Data using t-SNE. *Journal of Machine Learning Research* 9, 2579–2605.
40. Wattenberg, M., Viégas, F., and Johnson, I. (2016) How to Use t-SNE Effectively. *Distill*
41. Spiwok, V., and Kříž, P. (2020) Time-Lagged t-Distributed Stochastic Neighbor Embedding (t-SNE) of Molecular Simulation Trajectories. *Frontiers in Molecular Biosciences* 7, 132.
42. Chari, T., Banerjee, J., and Pachter, L. (2021) The Specious Art of Single-Cell Genomics. *bioRxiv*
43. Tiwary, P., and Berne, B. J. (2016) Spectral gap optimization of order parameters for sampling complex molecular systems. *Proceedings of the National Academy of Sciences* 113, 2839–2844.

44. Ghojogh, B., Ghodsi, A., Karray, F., and Crowley, M. Multidimensional Scaling, Sammon Mapping, and Isomap: Tutorial and Survey. 2020.
45. Tu, J. H., Rowley, C. W., Luchtenburg, D. M., Brunton, S. L., and Kutz, J. N. (2014) On dynamic mode decomposition: Theory and applications. *Journal of Computational Dynamics 1*, 391–421.
46. Klus, S., Nüske, F., Koltai, P., Wu, H., Kevrekidis, I., Schütte, C., and Noé, F. (2018) Data-Driven Model Reduction and Transfer Operator Approximation. *Journal of Non-linear Science 28*, 985–1010.
47. McInnes, L., Healy, J., and Melville, J. UMAP: Uniform Manifold Approximation and Projection for Dimension Reduction. 2020.
48. Trozzi, F., Wang, X., and Tao, P. (2021) UMAP as a Dimensionality Reduction Tool for Molecular Dynamics Simulations of Biomacromolecules: A Comparison Study. *The Journal of Physical Chemistry B 125*, 5022–5034, PMID: 33973773.
49. Tian, H., and Tao, P. (2020) ivis Dimensionality Reduction Framework for Biomacromolecular Simulations. *Journal of Chemical Information and Modeling 60*, 4569–4581.
50. Brunton, S. L., Proctor, J. L., and Kutz, J. N. (2016) Discovering governing equations from data by sparse identification of nonlinear dynamical systems. *Proceedings of the National Academy of Sciences 113*, 3932–3937.
51. Glielmo, A., Husic, B. E., Rodriguez, A., Clementi, C., Noé, F., and Laio, A. (2021) Unsupervised Learning Methods for Molecular Simulation Data. *Chemical Reviews 121*, 9722–9758, PMID: 33945269.
52. Kingma, D. P., and Welling, M. (2019) An Introduction to Variational Autoencoders. *Foundations and Trends® in Machine Learning 12*, 307–392.
53. Kingma, D. P., and Welling, M. Auto-Encoding Variational Bayes. 2014.

54. Sultan, M. M., Wayment-Steele, H. K., and Pande, V. S. (2018) Transferable Neural Networks for Enhanced Sampling of Protein Dynamics. *Journal of Chemical Theory and Computation* 14, 1887–1894.
55. Burgess, C. P., Higgins, I., Pal, A., Matthey, L., Watters, N., Desjardins, G., and Lerchner, A. Understanding disentangling in β -VAE. 2018.
56. Hernández, C. X., Wayment-Steele, H. K., Sultan, M. M., Husic, B. E., and Pande, V. S. (2018) Variational encoding of complex dynamics. *Phys. Rev. E* 97, 062412.
57. Ribeiro, J. M. L., Bravo, P., Wang, Y., and Tiwary, P. (2018) Reweighted autoencoded variational Bayes for enhanced sampling (RAVE). *The Journal of Chemical Physics* 149, 072301.
58. Mohanty, N., John, A. L.-S., Manmatha, R., and Rath, T. In *Handbook of Statistics*; Rao, C., and Govindaraju, V., Eds.; Handbook of Statistics; Elsevier, 2013; Vol. 31; pp 249–267.
59. Sultan, M. M., and Pande, V. S. (2018) Automated design of collective variables using supervised machine learning. *The Journal of Chemical Physics* 149, 094106.
60. Mendels, D., Piccini, G., Brotzakis, Z. F., Yang, Y. I., and Parrinello, M. (2018) Folding a small protein using harmonic linear discriminant analysis. *The Journal of Chemical Physics* 149, 194113.
61. Crammer, K., Dekel, O., Keshet, J., Shalev-Shwartz, S., and Singer, Y. (2006) Online Passive-Aggressive Algorithms. *Journal of Machine Learning Research* 7, 551–585.
62. Fisher, R. A. (1936) The use of multiple measurements in taxonomic problems. *Annals of Eugenics* 7, 179–188.
63. Capelli, R., Bochicchio, A., Piccini, G., Casasnovas, R., Carloni, P., and Parrinello, M. (2019) Chasing the Full Free Energy Landscape of Neuroreceptor/Ligand Unbinding by

- Metadynamics Simulations. *Journal of Chemical Theory and Computation* 15, 3354–3361.
64. Rizzi, V., Bonati, L., Ansari, N., and Parrinello, M. (2021) The role of water in host-guest interaction. *Nature Communications* 12, 93.
65. Tsai, S.-T., Kuo, E.-J., and Tiwary, P. (2020) Learning molecular dynamics with simple language model built upon long short-term memory neural network. *Nature Communications* 11, 5115.
66. Zeng, W., Cao, S., Huang, X., and Yao, Y. A Note on Learning Rare Events in Molecular Dynamics using LSTM and Transformer. 2021.
67. Lim, B., and Zohren, S. (2021) Time-series forecasting with deep learning: a survey. *Philosophical Transactions of the Royal Society A: Mathematical, Physical and Engineering Sciences* 379, 20200209.
68. Bhakat, S., and Söderhjelm, P. (2017) Resolving the problem of trapped water in binding cavities: prediction of host-guest binding free energies in the SAMPL5 challenge by funnel metadynamics. *Journal of Computer-Aided Molecular Design* 31, 119–132.
69. Pant, S., Smith, Z., Wang, Y., Tajkhorshid, E., and Tiwary, P. (2020) Confronting pitfalls of AI-augmented molecular dynamics using statistical physics. *The Journal of Chemical Physics* 153, 234118.
70. Pfaendtner, J., and Bonomi, M. (2015) Efficient Sampling of High-Dimensional Free-Energy Landscapes with Parallel Bias Metadynamics. *Journal of Chemical Theory and Computation* 11, 5062–5067.
71. Weininger, U., Modig, K., and Akke, M. (2014) Ring Flips Revisited: ¹³C Relaxation Dispersion Measurements of Aromatic Side Chain Dynamics and Activation Barriers in Basic Pancreatic Trypsin Inhibitor. *Biochemistry* 53, 4519–4525.

72. Kulkarni, M., and Söderhjelm, P. (2021) Free Energy Landscape and Rate Estimation of the Aromatic Ring Flips in Basic Pancreatic Trypsin Inhibitor Using Metadynamics. *bioRxiv*
73. Yu, C., Ma, X., Ren, J., Zhao, H., and Yi, S. Spatio-Temporal Graph Transformer Networks for Pedestrian Trajectory Prediction. 2020.